Wireless Networks
https://doi.org/10.1007/s11276-020-02268-5

An analytical framework for reliability evaluation of *d*-dimensional IEEE 802.11 broadcast wireless networks

Jing Zhao[1,2,3] · Zhijuan Li[1] · Yanbin Wang[4] · Zhuofei Wu[1] · Xiaomin Ma[5] · Yue Zhao[6]

Abstract
In this paper, we validate that the deterministic distance-based analytical model can be used to estimate the reliability of one-dimensional (1-D) 802.11 broadcast wireless networks compared with the interference-based analytical model. Therefore, we propose a deterministic distance-based reliability analytical framework for such networks in *d*-dimensional (*d*-D, $d \geq 1$) scenarios. This framework takes into account the fading channel and hidden terminal problem and makes three commonly used reliability metrics able to be resolved, including point-to-point packet reception probability (*NRP*), packet delivery ratio (*PDR*), and packet reception ratio (*PRR*). There are two key factors involved in deducing the effect of hidden terminals. One is to measure the hidden terminal transmission probability during the vulnerable period, which can be calculated based on the approximate solution of the semi-Markov process model capturing the channel contention and the back-off behavior. Another is the challenge to determine the size of the area to which the hidden terminals belong. First, we give a general mathematical expression on the size of the hidden terminal coverage affecting *NRP* which is an important part of the closed-form solution of *NRP*/*PRR*. Second, we adopt the Monte-Carlo method to solve the size of general hidden terminal coverage affecting *PDR*, making it possible to approximate *PDR*, as well as control the efficiency and accuracy by constraining the relative error. Finally, we adopt a multi-parameter optimization scheme to find the optimum settings for the network to ensure the quality of service and maximize channel utilization. A series of experimental results show that the framework can be used to access the reliability of 802.11 based *d*-D broadcast wireless network and pave the way for further optimization.

Keywords Reliability evaluation · *d*-D broadcast wireless networks · Fading channel · Hidden terminal problem · Monte-Carlo method

✉ Jing Zhao
zhaoj9988@dlut.edu.cn

✉ Yanbin Wang
wangyb@hit.edu.cn

✉ Xiaomin Ma
xma@oru.edu

[1] Department of Computer Science and Technology, Harbin Engineering University, Harbin 150001, China

[2] School of Software Technology, Dalian University of Technology, Dalian 116024, China

[3] Cyberspace Security Research Center, Peng Cheng Laboratory, Shenzhen 518052, China

[4] Department of Industrial Engineering, Harbin Institute of Technology, Harbin 150001, China

[5] College of Science and Engineering, Oral Roberts University, Tulsa, OK 74171, USA

[6] Science and Technology on Communication Security Laboratory, Chengdu 610041, China

Published online: 06 February 2020

1 Introduction

Recently, many wireless networks such as wireless sensor networks (WSNs) [1], vehicular ad hoc networks (VANETs) [2], LTE cellular networks [3], and unmanned aerial vehicular (UAV) networks [4, 5] extensively provide one-hop and multi-hop broadcast services for various applications such as medical monitoring [6], safety services [7], and military field communication [8], etc. These networks are built on different geometric space. For example, we usually abstract vehicles communication system on the highway as 1-D VANET, take the evolved multimedia broadcast multicast service (eMBMs) or device-to-device (D2D) service in LTE cellular networks working on two-dimensional (2-D) cell, and ad hoc networks for UAV are naturally three-dimensional (3-D). However, the broadcast nodes may face many disturbances such as fading channel and the well-known hidden terminal problem, which can cause performance degradations. The link reliability of MAC layer has obtained more attention from the researchers, who have been seeking to access the wireless broadcast system from multiple perspectives and suggest improvements for different applications. Currently, *NRP*, *PDR*, and *PRR* are three commonly used MAC layer reliability metrics [9], *NRP* represents the probability that a node within the transmission range of the sender successfully receives a packet. *PDR* evaluates the likelihood that all intended receivers successfully receive a packet. *PRR* depicts the percentage of receivers that successfully receive a packet from the sender.

Compared with the simulation method [10], the theoretically analytical model can save much time and is better for evaluating the reliability of the network. A few analytic models have been used to evaluate *NRP*/ *PDR*/*PRR* of 1-D broadcast mobile ad hoc networks (MANETs) [11–17]. Various approaches have been deployed in these papers to investigate the impact of IEEE 802.11 channel access, the impact of the fading channel, and the impact of the hidden terminal problem. Most recently, a new interference-based model for the analysis of QoS and capacity was proposed for 1-D VANET safety message broadcast scenario [18, 19]. Considering the fading channel and hidden terminal problem, the model regarded the packet whose signal-to-interference ratio (SIR) is higher than the threshold at the receiver as a successful reception, which is closer to the principle of a physical system [20–22].

However, most of the network configurations cannot be abstracted by 1-D models. *NRP*/*PRR* evaluation accounting for the impact of fading channel and collisions in general 2-D wireless ad hoc broadcast networks has been recently addressed and derived [23]. Recently, Ma et al. [24] built the theoretical model for *NRP*/*PDR*/*PRR* of one-hop broadcasting service in the general *d*-D broadcast wireless networks. However, they took channel fading as the only factor causing broadcast failures and ignored the impact of hidden terminal problem through assuming the collisions from different nodes' transmissions can be neglected if the overall transmission rate is very small compared to the channel capacity or perfect channel access protocol is applied. Up to the present time, *PDR* with the impact of hidden terminal problem has not been given in the case of 2-D or higher dimension.

This article extends [24] and proposes a more accurate analytical framework for one-hop broadcasting service of *d*-D 802.11 wireless networks by considering both fading channel and hidden terminal problem. During the period that the packet travels from the sender to the receiver, not only the hidden terminal may interfere with packet reception at the receiver, but also the nodes in the carrier sensing range of the sender, who may transmit concurrently in the same slot with the sender, can make the reception fail. We do not consider the impact of concurrent transmission, which could be neglected compared with that of the hidden terminal problem [9]. This proposed framework adopts the deterministic distance-based analytical model to measure the effect of the hidden terminals, which are limited to the nodes whose transmissions can fail receiving nodes. Then, the evaluation is converted to measure the hidden terminal transmission probability during the vulnerable period [13] and solve the size of the area to which the hidden terminals belong. The SMP model [13], which is a general approach to capture the channel contention and the back-off behavior, has been developed to calculate the hidden terminal transmission probability. How to solve the size of the hidden terminal coverage needs to be studied.

The size of hidden terminal coverage affecting *NRP* can be determined by a closed-form mathematical expression based on the distance between the sender and the receiver. The hidden terminal coverage affecting *PDR* is an irregular area which is defined as the overall interference area from all the one-hop receivers excluding the carrier sensing area of the sender [9]. [25] provided an efficient algorithm solving the area of hidden terminal coverage affecting *PDR* for a static 2-D network scenario. The algorithm could not address the volume of the 3-D irregular area due to the different geometric characteristics. Thus we adopt the MC method to evaluate the size of the hidden terminal coverage affecting *PDR*. Furthermore, we control the efficiency and accuracy of the MC method based on the statistical characteristics between the number of samples and the relative errors. At the same time, the number of sampling points is further reduced by adaptively select the minimum sample area.

Because the wireless broadcast network environment is various and the reliability requirements of the different

applications are also different, the optimum transmission settings may vary. In [26], we adopted the conventional Particle Swarm Optimization (PSO) based algorithm, which dynamically adjusts the combination of transmission parameters of VANET, let the application-level reliability meet the requirements of safety applications, and then approach the transmission capacity. In this paper, we refine the optimization scheme of [26] to keep relatively high reliability and QoS constraint transmission capacity in a dynamically changing environment.

Now we highlight the major contributions of our paper:

(1) We compare the interference-based analytical model with the deterministic distance-based analytical model in various scenarios with general densities and general data rates. The deterministic distance-based analytical method is verified to be accurate enough and reasonable.
(2) We propose a general reliability analytical framework evaluating *NRP*/*PDR*/ *PRR* for 802.11 based *d*-D wireless broadcast networks. The framework, considering the fading channel and the hidden terminal problem, helps managers assess network capabilities and properly configure the network.
(3) We present the generalized mathematical expressions of *NRP*/*PRR* with the hidden terminal problem by solving the size of the hidden terminal coverage affecting *NRP*. These developed expressions are the function of the receiver's distance to the sender. They are useful for studying the effects of hidden terminals at different receiving distances.
(4) We evaluate the approximation of *PDR* via adopting the MC method to calculate the size of the general hidden terminal coverage affecting *PDR*. The efficiency and accuracy of the MC method can be controlled by applying the relationship between the number of samples and the relative errors.
(5) We apply a multi-parameter optimization approach based on Bare-Bones Particle Swarm Optimization (BBPSO) to adjust the communication settings of the networks. The optimal combination of parameters can be found taking into account the state of the network, ensuring reliability and maximizing utilization.

To make this paper more readable, we summary the symbols in Table 1. The rest of this paper is summarized as follows. In Sect. 2, we describe the related work, including the system assumptions for the broadcast scenario, the reliability metrics, the hidden terminal problem analysis, and the comparisons between the interference-based model and the deterministic distance-based model. In Sect. 3, the derivations of *NRP*/*PDR*/*PRR* for *d*-D broadcast wireless networks are gradually unfolding. Section 4 describes the multi-parameter optimization problem and the refined optimization algorithm based on BBPSO. In Sect. 5, we conduct a series of experiments to validate the efficiency of the proposed reliability analytical framework with the multi-parameter optimization scheme. At the same time, we also discuss how to balance the efficiency and the accuracy of the MC method. Finally, Sect. 6 concludes this paper.

2 Related work

2.1 System model and assumptions

Figure 1 represents the general system model for IEEE 802.11 *d*-D broadcast wireless networks. Broadcast does not adopt the scheme named "Request To Send/Clear To Send (RTS/CTS)" [27], which can inform surrounding nodes about the transmission to avoid the conflict caused by the simultaneous arrival of packets. According to the specification of IEEE 802.11p, Distributed Coordination Function (DCF) [28] is responsible for coordinating the channel access by taking carrier sense multiple access with collision avoidance (CSMA/CA) mechanism in the MAC layer. We make several assumptions about the system model.

(1) Given that all broadcast nodes are randomly distributed in the *d*-D geometry space according to a homogeneous *d*-D Poisson distribution [24, 29]. β is the density, the probability of finding k nodes in the network area A is expressed as follows:

$$Pr(k,A) = e^{(-\beta S(A))}\frac{(\beta S(A))^k}{k!} \quad (1)$$

where $S(A)$ represents the size of network area A.
(2) All nodes have the same transmission range of R, as shown in Fig. 1. It is defined as the maximum distance that a packet can be successfully received. It depends on the transmission power and the fading channel.
(3) All nodes have equal carrier sensing range R_{cs} and $R \le R_{cs}$. R_{cs} is the average carrier sensing range in which the nodes can detect the transmission from the *sender* [19, 30]. As shown in Fig. 1, during the *broadcasting* period of the *sender*, the *receiver*/*suppressed* would not transmit until the end of this transmission because it senses that the channel is busy.
(4) All nodes have equal interference range R_{int}. We have $R \le R_{int} \le R_{cs}$ because the signal not reaching the receiving threshold may still have an impact on the normal receiving [31]. As shown in Fig. 1, the

Table 1 Summary of symbols

Symbols	Descriptions
d	Geometric space dimension
R	Transmission range (m)
R_{cs}	Carrier sensing range (m)
R_{int}	Interference range (m)
r	Receiving range (m)
x	Receiving distance (m) between the sender and the receiver
β	Nodes density
λ	Packet generation rate of each node (packets/s)
W	IEEE 802.11 CSMA back-off window size
$DIFS$	Distributed interframe space
δ	Propagation delay
T_H	Packet header transmission time (MAC layer header + PHY layer header)
T_e	Transmission time of one packet
$2T_e$	Vulnerable period in which collisions occur if hidden terminals transmit
π_{XMT}	Steady-state probability that one node is in transmission state
T_p	Sojourn time that one node is in transmission state
p_t	Hidden terminal transmission probability during the vulnerable period
PA	Packet length
R_d	Data rate
γ	Path loss exponent
m	Fading parameter
H_1	Hidden terminal coverage affecting NRP
S_1	The size (area or volume) of H_1
$H_{\sum}$	Hidden terminal coverage affecting PDR in one scenario
$S_{\sum}$	The size (area or volume) of $H_{\sum}$
$H^g_{\sum}$	General hidden terminal coverage affecting PDR
$S^g_{\sum}$	The size (area or volume) of $H^g_{\sum}$
L_S	Side length of sampling area
p	The probability that one sampling point falls in the sampling area
X_α	Confidence level
ϵ_s	Relative error of multi trials
ϵ_p	Relative error of p in one trial
e	Predefined relative error
M_e	Number of sampling points for relative error e in one trial
n_e	Number of trials for relative error e
M_{avg}	Average number of sampling points in n_e trials
T_1	Execution time of one trial
$T_{\sum}$	Total execution time of n_e trials
N_{ROI}	Number of nodes in the region of interest
Δ	PRR threshold
$\boldsymbol{X}$	Position of a BBPSO particle
$\boldsymbol{X}^{(k)}_{i,pbest}$	Best historical location of the ith particle in the kth iteration
$\boldsymbol{X}^{(k)}_{gbest}$	Best historical global location of BBPSO

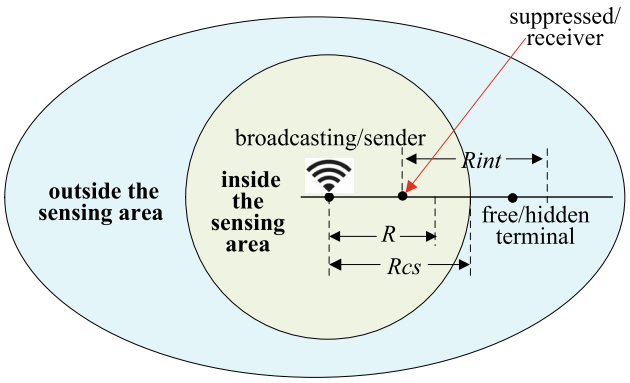

Fig. 1 The general system model for IEEE 802.11 *d*-D broadcast wireless networks

hidden terminal/free, beyond the sensing range of the *sender* but within the interference range of the *receiver*, may transmit a packet which can reach the *receiver* during the broadcasting period of *sender* and cause a failure to receive at the *receiver*.

(5) At each node, the time interval between the arrival of two consecutive packets follows Exponential distribution with the rate λ (in packets per second).

(6) The queue length of packets at each node is unlimited. Therefore, each node can be modeled as a discrete-time Markov arrival/General service distribution/1 service channel (M/G/1) queue.

(7) Based on the former research [32, 33], *Nakagami* fading model, which was proposed by matching the empirical results, can better describe the actual imperfect channel where signal attenuation and path loss occur. Therefore, we adopt the *Nakagami* propagation model to describe the impact of the fading channel in this paper.

(8) We do not consider the impact of node mobility on the reliability since the node is almost stationary within one packet transmission duration, which is usually less than 1 ms [30].

2.2 Reliability metrics

In this paper, we research the three reliability metrics: *NRP*, *PDR*, and *PRR*. They could measure the reliabilities of the network from different perspectives.

(1) *NRP* is defined as the probability that a node within the transmission range of the sender successfully receives a packet, which can be measured as

$$NRP(x) = \frac{\text{No. of packets received successfully by the node}}{\text{Total no. of packets transmitted to the node}} \tag{2}$$

where x is the distance between the sender and the receiver. Sometimes, we only concern the connectivity of the link between two nodes in the case that the message is dedicated to a specific node. Therefore, *NRP* is used as a reliability index for such applications.

(2) *PDR* can evaluate how a packet from a sender is received by all intended receivers. It is defined as the ratio of the number of packets successfully by all receivers to the number of packets transmitted. The expression is:

$$PDR(r) = \frac{\text{No. of packets received by all nodes within distance } r \text{ from the sender}}{\text{No. of packets sent by the sender}} \tag{3}$$

where r is the distance from the sender. Usually, the sender broadcasts a packet to the surrounding nodes within a circular transmission range of the sender, all of which are the intended receivers of the packet. A reception may be a failure due to the channel fading and hidden terminal problem. However, some applications require all packets generated during the given time window to be delivered successfully to all neighbors because these packets make up a complete and important message. So, *PDR* is used as a reliability index in this case.

(3) *PRR* [10] is defined as the percentage of nodes that successfully receive a packet from the sender among the receivers at the moment that the packet is sent out. The expression of *PRR* is:

$$PRR(r) = \frac{\text{No. of nodes within distance } r \text{ receiving a packet from the sender}}{\text{Total no. of nodes within distance } r \text{ from the sender}} \tag{4}$$

where r is the receiving range from the sender. Certain messages are dedicated to some nodes rather than to all neighbors, for example, brake action should be delivered to the vehicles in the rear direction in time, not to the vehicles in all directions. Therefore, these applications are more inclined to take the average link connectivity consideration by evaluating how many nodes can receive the message successfully. Furthermore, *PRR* provides a deeper insight into the reliability as the range changes because it is a function of the receiver's distance to the sender.

2.3 Hidden terminal problem analysis

A packet transmission time equals that the time instant in which it is entirely received minus the time instant in which it leaves the queue of the node. We can theoretically calculate the transmission time (denoted by T_e), which is made up of the packet header transmission time, the packet body transmission time and the propagation delay δ. It is expressed as:

$$T_e = T_H + E[PA]/(R_d \times 10^6) + \delta \tag{5}$$

where T_H is the packet header transmission time including physical layer header and MAC layer header, $E[PA]$ is the mean of packet size PA, R_d represents the data rate (Mbps).

The packet transmission time is the same as each other by assuming that all nodes adopt the same data rate to broadcast an equal size packet. Therefore, the hidden terminal vulnerable period, as shown in Fig. 2, in which the hidden terminal transmissions can cause interference is two times the transmission time, including one T_e just before the transmission of the sender and another T_e just after the transmission of the sender.

Furthermore, [13] built the SMP model, through which we can obtain the solution of the hidden terminal transmission probability p_t during the vulnerable period.

$$p_t = \pi_{XMT}\frac{2T_e}{T_p} = \pi_{XMT}\frac{2(T_p - DIFS)}{T_p} \tag{6}$$

where T_p is the mean sojourn time in transmission state (denoted by XMT), $T_p = T_e + DIFS$, $DIFS$ represents the distributed interframe space, and π_{XMT} represents the steady-state probability that a node is in XMT state, which can be expressed as follows:

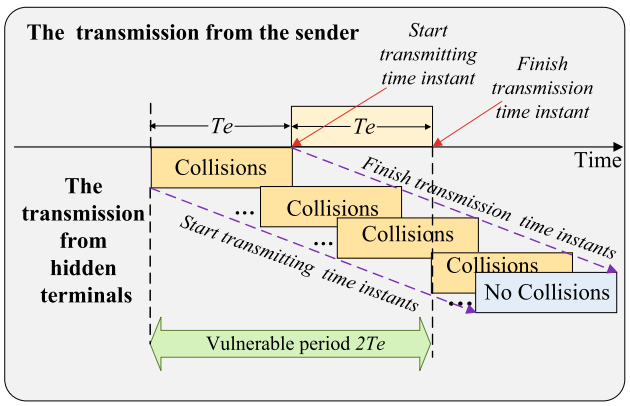

Fig. 2 Hidden terminal vulnerable period

$$\begin{aligned}
\pi_{XMT} &= \frac{2T_p}{A + 2T_p + 2B} \\
A &= [\rho + q_b(1-\rho)]\left[(\sigma + p_b T_p)W + (\sigma - p_b T_p)\right] \\
B &= (1-\rho)(1/\lambda + DIFS)
\end{aligned} \tag{7}$$

where σ is time duration of one back-off slot, W is the back-off window size, ρ is the probability that there are packets in the queue of the tagged node, q_b is the probability that the channel is detected busy in DIFS time by the tagged node, and p_b is the probability that it senses channel busy during one back-off time slot.

$$\begin{aligned}
p_b &= 1 - (1 - P_{XMT})^{N_{tr}} \\
P_{XMT} &= \frac{1}{W}\frac{T_p - DIFS + 2\sigma}{T_p}\pi_{XMT} + \left(1 - \frac{1}{W}\right)\frac{2\sigma}{T_p}\pi_{XMT} \\
q_b &= 1 - (1 - p_b)^{\frac{T_p W}{T_p - DIFS + 2\sigma W}}
\end{aligned} \tag{8}$$

where P_{XMT} is the probability that a neighbor's transmission is detected by the tagged node in a back-off time slot, and N_{tr} is the number of nodes in the sensing range of the sender.

Equations (7) and (8) show that q_b can be expressed in terms of p_b, and p_b depends on ρ and itself. Whereas ρ is function of p_b because it depends on the mean service time to transmit a packet. That is, ρ and p_b are interacting. Therefore, we adopt the fixed-point iteration method described in [13] to determine ρ and p_b, then approximate π_{XMT}. The fixed-point iteration method, starting with an initial saturation condition $\rho = 1$, is terminated when the difference between successive ρ is below a certain tolerance level after several iterations. In each iteration, ρ is updated to the ratio of the packet generation rate to the service rate when the system is in steady state, otherwise 1. The existence, uniqueness, and convergence of this method have been proved [13].

2.4 Comparisons between the interference-based model and the deterministic distance-based model

We compare *NRP*s/*PDR*s/*PRR*s of the interference-based model [18, 19] and the deterministic distance-based model and observe their difference. We design three nodes densities (0.02 nodes/m for low density, 0.1 nodes/m for medium density, and 0.18 nodes/m for high density) at each data rate (3 Mbps, 6 Mbps, 12 Mbps, and 24 Mbps) as the scenarios with different interferences. We write a Python program to implement the deterministic distance-based model [13], as well as developing a C++ parallel

Table 2 Relationship of Modulation Schemes, R_ds,and SINR thresholds for IEEE 802.11p in NS2.35

Modulation Scheme	R_d (Mbps)	SINR threshold
BPSK 1/2	3	3.1623
QPSK 1/2	6	6.3096
16QAM 1/2	12	31.6228
64QAM 2/3	24	316.2278

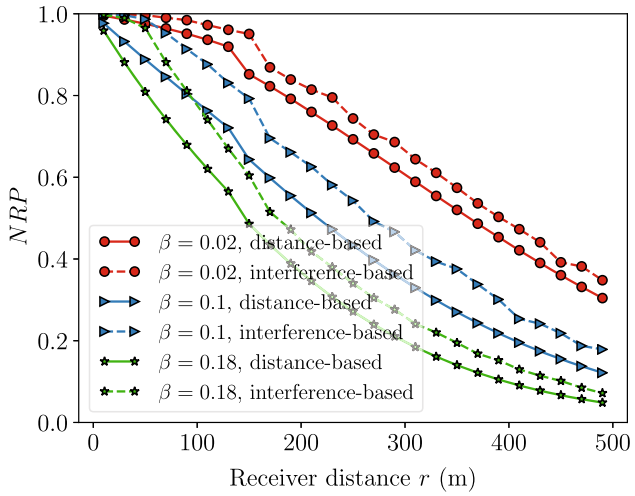

Fig. 3 *NRP* comparisons of the two models with the data rate of 3 Mbps

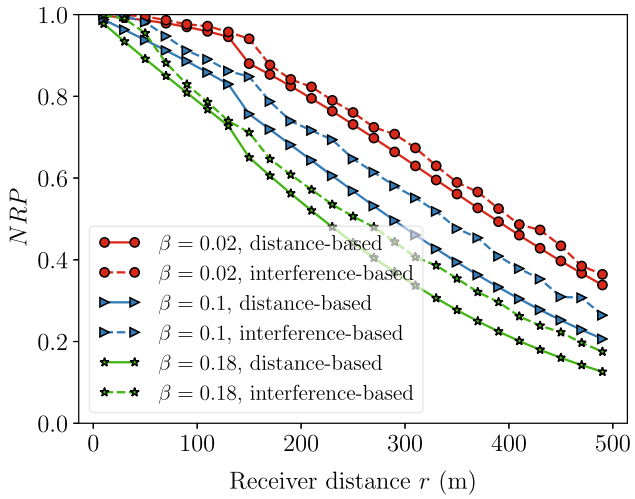

Fig. 4 *NRP* comparisons of the two models with the data rate of 6 Mbps

program for the interference-based model. We adopted the signal-to-interference-plus-noise ratio (SINR) thresholds in NS2.35 as the SIR thresholds in our experiments, as shown in Table 2.

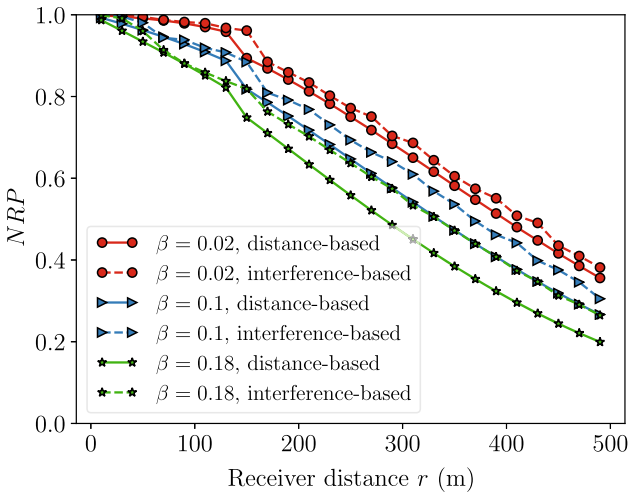

Fig. 5 *NRP* comparisons of the two models with the data rate of 12 Mbps

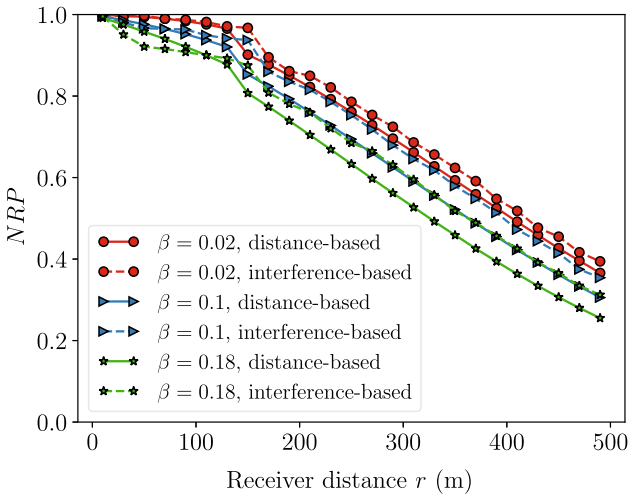

Fig. 6 *NRP* comparisons of the two models with the data rate of 24 Mbps

Figures 3, 4, 5 and 6 show the *NRP*s of the two models with the data rate of 3 Mbps, 6 Mbps, 12 Mbps, and 24 Mbps. The solid line draws the calculation results of the deterministic distance-based model. The dotted line represents the theoretical results of the interference-based model. It can be observed that *NRP*s calculated by the two models are very consistent. Therefore, the deterministic distance-based model can be used in the network scenario.

We could find that the interference-based analytical model yields better reliability because some packets may be received successfully when the hidden terminals transmit during the vulnerable period. We can further observed that the discrepancy between the two models at the data rate of 24 Mbps is less than that at the data rate of 12 Mbps, which is then less than that at the rate of 6 Mbps, and it is maximum at the data rate of 3 Mbps. The hidden terminals

have more chances to occupy channels during the vulnerable period when the data rate is low, and this increases the collision probability. At the same time, the SINR threshold at a low data rate is less than that at a high data rate. The above two conditions increase the possibilities that the failure reception based on the deterministic distance model is considered successful in the interference-based model. Besides, *PDR* and *PRR* results yield conclusions similar to *NRP*, which are shown in Appendix A because of the space problem.

3 The reliability analytical framework

In our model, a successful reception requires fitting two conditions. The received power is greater than the reception threshold (*RT*), and none of the packets from other senders arrive at the receiver until the packet is received successfully. The two conditions are independent of each other; therefore, we would consider the impact of the fading channel and the hidden terminals on the reliability separately.

3.1 *NRP* evaluation

3.1.1 The impact of the hidden terminals

As shown in Fig. 7, we place a transmitting node O at the origin, one receiver T on the X-axis, and the distance between O and T is x. The shaded area (denoted by H_1) represents the hidden terminal coverage affecting *NRP* in which the transmissions of nodes can interfere with T receiving the packets from O. Denote $NRP_H(x)$ as the *NRP* considering the impact of hidden terminals. According to the definition of *NRP*, $NRP_H(x)$ equals the probability that all hidden terminals do not start to transmit a packet during the vulnerable period, and it can be expressed as

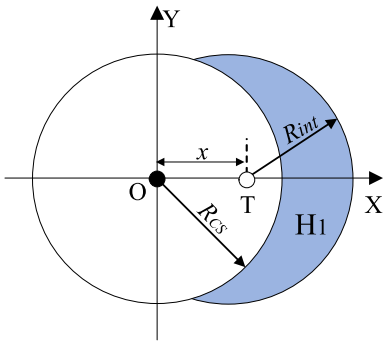

Fig. 7 Hidden terminal coverage affecting *NRP* H_1

$$\begin{aligned} NRP_H(x) &= \sum_{i=0}^{\infty}(1-p_t)^i Pr(i,H_1) \\ &= \sum_{i=0}^{\infty}(1-p_t)^i \frac{(\beta S_1(x))^i}{i!} e^{-(\beta S_1(x))} \\ &= \exp(-p_t \beta S_1(x)) \end{aligned} \tag{9}$$

where p_t is the hidden terminal transmission probability during the vulnerable period, $S_1(x)$ is the size of H_1, and it can be derived from that the volume of d-D sphere with a radius of R_{int} minus intersection volume of two spheres with distance x. The intersection is composed of two spherical caps which have a common cap base. The distance between the sender and the cap base is $|c_1|$, the distance from the receiver to the cap base is $|c_2|$, and we have

$$c_1 = \frac{x^2 + R_{cs}^2 - R_{int}^2}{2x}; c_2 = \frac{x^2 - R_{cs}^2 + R_{int}^2}{2x}$$

Therefore, the generalized expression of $S_1(x)$ for any dimension is evaluated as [34].

$$S_1(x) = V_d(R_{int}) - V_d^{cap}(R_{cs}, c_1) - V_d^{cap}(R_{int}, c_2) \tag{10}$$

where the volume of a sphere for a given radius R_g is expressed as

$$V_d(R_g) = \frac{\pi^{d/2}}{\Gamma(d/2+1)} R_g^d$$

where $\Gamma()$ is the standard Gamma function, and the volume of a spherical cap for a given radius R_g is evaluated as

$$V_d^{cap}(R_g, c \geq 0) = \frac{1}{2}\frac{\pi^{d/2}}{\Gamma(d/2+1)} R_g^d I_{1-c^2/R_g^2}\left(\frac{d+1}{2}, \frac{1}{2}\right)$$

$$V_d^{cap}(R_g, c < 0) = \frac{\pi^{d/2}}{\Gamma(d/2+1)} R_g^d - V_d^{cap}(R_g, -c)$$

and the regularized incomplete beta function is given by

$$I_y(a,b) = \frac{\int_0^y t^{a-1}(1-t)^{b-1}dt}{\int_0^1 t^{a-1}(1-t)^{b-1}dt}$$

3.1.2 The impact of the fading channel

$NRP_F(x)$ represents the *NRP* taking the impact of *Nakagami* fading channel into consideration, and it equals the probability that a packet is received successfully in the absence of interference. As a result of [35], the expression is given via calculating the probability that the received power is greater than the reception threshold, which represents the average power at the transmission range R. Then, $NRP_F(x)$ is as follows:

$$NRP_F(x) = 1 - \frac{m^m}{\Gamma(m)} \int_0^{(x/R)^\gamma} z^{m-1} e^{-mz} dz \tag{11}$$

where $\Gamma()$ is the standard Gamma function, m is the fading parameter in the given receiving distance, γ is the path loss exponent which is usually empirically determined by field measurements.

Therefore, the evaluation of NRP can be combined as follows.

$$NRP(x) = NRP_H(x) \times NRP_F(x) \tag{12}$$

where x is the distance between the sender and the receiver.

3.2 *PDR* evaluation

3.2.1 The impact of the hidden terminals

In d-D broadcast wireless networks, the number and locations of nodes are random. Figure 8 presents four possible scenarios, each with the different number of nodes in the range r from the sender. In one subfigure, the origin O is the sender transmitting packets, T_i $(i \geq 1)$ receives a packet from O, less than r $(r \leq R)$ from O. The shaded area marked by $H_{\sum}$, in which the transmissions of nodes would interfere with at least one receiver receiving the packets from O, is all T_i $(i \geq 1)$'s total interference coverage with range R_{int} excluding O's carrier sensing coverage with range R_{cs}. Therefore, $H_{\sum}$ is regarded as the hidden terminal coverage affecting PDR, and it is formally expressed as follows.

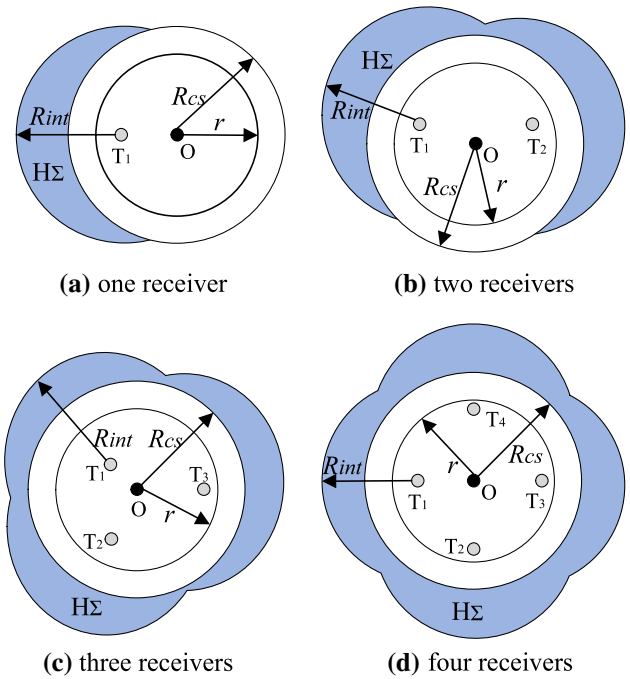

Fig. 8 Hidden terminal coverage affecting PDR $H_{\sum}$ in different scenarios

$$H_{\sum}(r) = \bigcup_{i=1}^{T_r} C(T_i, R_{int}) \bigcap \overline{C}(O, R_{cs}) \tag{13}$$

where T_r is the number of nodes within the distance r from the sender, $C(O, l)$ denotes the coverage of range l centered at O, $\overline{C}$ is complement of C.

Since the network scenario is changing, the general hidden terminal coverage affecting PDR is represented by $H^g_{\sum}$ whose size is the mean of $H_{\sum}$ in all scenarios. In line with the definition of PDR, PDR with the impact of the hidden terminals, in terms of $PDR_H(r)$, equals the probability that all hidden terminals do not start to transmit packet during the vulnerable period. So, $PDR_H(r)$ can be expressed as

$$\begin{aligned} PDR_H(r) &= \sum_{i=0}^{\infty} (1-p_t)^i Pr(i, H^g_{\sum}) \\ &= \sum_{i=0}^{\infty} (1-p_t)^i \frac{(\beta S^g_{\sum}(r))^i}{i!} e^{-(\beta S^g_{\sum}(r))} \\ &= \exp(-p_t \beta S^g_{\sum}(r)) \end{aligned} \tag{14}$$

where β is the nodes density, $S^g_{\sum}$ is the size of $H^g_{\sum}$, and it has no closed-form solution. We take the size of $H_{\sum}$ as a random variable, in terms of $S_{\sum}$. Then we perform multi simulation trials to construct network scenarios that cover sufficient patterns, then evaluate $S_{\sum}$ using MC method in each trial. $S^1_{\sum}, S^2_{\sum}, S^3_{\sum}, \ldots, S^n_{\sum}$ are samples of $S_{\sum}$ in a total of n trials. The mean $\overline{S_{\sum}}$, as shown in the Eq. (15), is an estimate of $S^g_{\sum}$.

$$\overline{S_{\sum}} = \frac{1}{n} \sum_{i=1}^{n} S^i_{\sum} \tag{15}$$

Description of the trial Given that the nodes follow the Poisson process with the density β. First, we place a node on the origin O as the sender and generate other broadcasting nodes in d-D coordinates according to the Poisson process algorithm described in [36]. The network area

where nodes are placed is large enough to ensure randomness. Second, we pick the nodes T_is within the range r from the sender to determine the hidden terminal coverage according to the Eq. (13). Third, we adopt the MC method to evaluate $S_{\sum}$ by evenly placing sampling points in the sample area SA, which is a square or cube with side length of L_S. In each trial, we choose the minimum sample area whose side length L_S can be written as:

$$L_S = 2(max(||T_iO||) + R_{int}), \quad i = 0, 1, 2, ..., T_r \tag{16}$$

where $||T_iO||$ is the distance from T_i to O, R_{int} is the interference range, and T_r is the number of nodes within the receiving range r of the sender. The probability p $(0 \le p \le 1)$ of the sampling points dropping in $H_{\sum}$ is the statistic, which is the ratio of the number of sampling points dropping in $H_{\sum}$ to the total number of sampling points. p is also equal to the ratio of $S_{\sum}$ to the size of SA. Therefore, $S_{\sum}$ is written as pL_S^d $(d \in [2, 3])$.

Evaluate the number of trials n_e The standard deviation of the sample mean value [37] is denoted by $\sigma\left(\overline{S_{\sum}}\right)$, and $\sigma\left(\overline{S_{\sum}}\right) = \sigma(S_{\sum})/\sqrt{n}$, where $\sigma(S_{\sum})$ is the standard deviation of the sample. Table 3 lists the relationship between significant level, confidence level, and the normal difference in terms of the three-sigma rule. The relative error with the given confidence level is

$$\varepsilon_s = \frac{X_\alpha \sigma\left(\overline{S_{\sum}}\right)}{\overline{S_{\sum}}} = \frac{X_\alpha \sigma\left(S_{\sum}\right)}{\overline{S_{\sum}}\sqrt{n}} \tag{17}$$

where n is the number of trials. Therefore, in the case of the given relative error e and the confidence level, the number of trials n_e can be evaluated as follows:

Table 3 Relationship between significant level, confidence level and the normal difference

Significant level α	Confidence level $1-\alpha$	Normal difference X_α
0.3173	0.6827	1.0
0.0455	0.9545	2.0
0.0027	0.9973	3.0

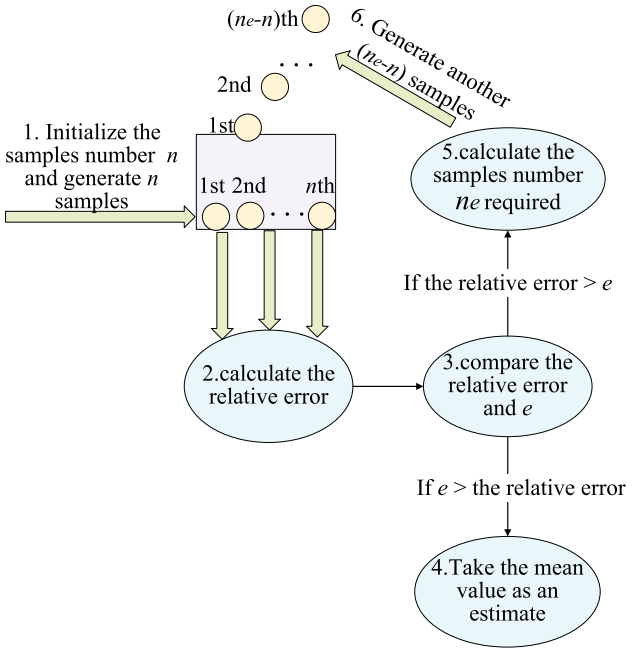

Fig. 9 Evaluate $S_{\sum}^g(r)$ with n_e trials

$$n_e = \left(\frac{X_\alpha \sigma(S_{\sum})}{e\overline{S_{\sum}}}\right)^2 \tag{18}$$

Evaluate $S_{\sum}^g(r)$ ***with*** n_e ***trials*** Fig. 9 shows the process of evaluating $S_{\sum}^g(r)$ with n_e trials. We describe these steps as follows.

(1) Initialize the number of trials n and the predefined relative error e;
(2) Generate n individual samples via trials;
(3) Calculate the relative error ε_s of n samples according to the Eq. (17);
(4) If $\varepsilon_s \le e$, the sample mean value is considered to be an estimate of $S_{\sum}^g(r)$;
(5) If $\varepsilon_s > e$, calculate the samples number n_e required using the Eq. (18). Then, we regenerate another $(n_e - n)$ samples, and recalculate the relative error of total n_e samples;
(6) Continue the steps (4)–(5) until the relative error ε_s is not greater than e.

Evaluate p ***for each trial*** Because the sample area SA is a square or cube with side length of L_S centered on the

sender, therefore, the coordinates (x_i, y_i, z_i) of sampling points are

$$\begin{cases} x_i = \pm\left(\frac{L_S}{2}\right)\xi; & y_i = \pm\left(\frac{L_S}{2}\right)\xi \\ z_i = \pm\left(\frac{(d-2)L_S}{2}\right)\xi, & d \in [2,3] \end{cases} \tag{19}$$

where ξ is a uniformly distributed random number in (0,1). According to the Eq. (13), a sampling point drops in $H_{\sum}$ when the following two conditions are satisfied.

- The distance from the sampling point to the sender is greater than R_{cs};
- Exist a receiver with the distance from the sampling point less than R_{int}.

Therefore, we design the random variable $p(x_i, y_i, z_i)$ as follows

$$p(x_i, y_i, z_i) = \begin{cases} 1, & \text{if } i\text{th sampling point is in } H_{\sum} \\ 0, & \text{else} \end{cases}$$

Assuming there are M sampling points, the mean value $\bar{p}$ and the standard derivation $\sigma(p)$ are

$$\bar{p} = \frac{1}{M}\sum_{i=1}^{M} h(x_i, y_i, z_i); \quad \sigma(p) = \sqrt{\bar{p}(1-\bar{p})} \tag{20}$$

Given the relative error e and the confidence level, the same method is used to determine the number of sampling points required. Therefore, the estimation process for p is as follows:

(1) Initialize the number M of sampling points and the predefined relative error e;
(2) Generate M sampling points according to the Eq. (19);
(3) Calculate the relative error ε_p with the given confidence level:

$$\varepsilon_p = \frac{X_\alpha \sigma(p)}{\bar{p}\sqrt{M}} = X_\alpha \sqrt{\frac{1-\bar{p}}{\bar{p}M}} \tag{21}$$

(4) If $\varepsilon_p \le e$, the mean value is taken as an estimate of p;
(5) If $\varepsilon_p > e$, calculate the number M_e of sampling points required according to the Eq. (22). Therefore, we regenerate another $(M_e - M)$ sampling points, and recalculate the relative error of a total M_e sampling points;

$$M_e = (X_\alpha)^2 \frac{1-\bar{p}}{e^2\bar{p}} = \frac{(X_\alpha)^2}{e^2}\left(\frac{1}{\bar{p}} - 1\right) \tag{22}$$

(6) Continue the steps (4)–(5) until the relative error is not greater than e.

Algorithm 1 The process of solving $S^g_{\sum}(r)$

Input: d, R_{cs}, R_{int}, r
Output: $S^g_{\sum}(r)$

```
trial times k ← 0
evaluate the number of trials n_e (see Fig. 9)
while k < n_e do
    increment k ← k + 1
    place the sender on the origin O
    generate other broadcasting nodes according to the Poisson process
    for each node a in allBroadcastingNodes do
        if ||a − O|| < r then
            append this node into listOfReceivers
        end if
    end for
    evaluate M_e^k (similar to Fig. 9)
    generate M_e^k uniformly distributed sampling points in the sample area SA
    for each point b in allSamplingPoints do
        if ||b − O|| < R_cs then
            continue
        else
            for each node c in listOfReceivers do
                if ||b − c|| < R_int then
                    increment points number in the hidden terminal coverage ht ← ht + 1
                    break
                end if
            end for
        end if
    end for
    p ← ht/M_e^k; S^k_∑(r) ← pL_S^d
    increment S^g_∑(r) ← S^g_∑(r) + S^k_∑(r)
end while
return S^g_∑(r) ← S^g_∑(r)/n_e
```

The execution time analysis Algorithm 1 describes the overall process of solving $S^g_{\sum}(r)$. The overall process includes n_e trials with M_e^k sampling points in the kth trial. In the kth trial, there will be generating broadcasting nodes, picking the receiving nodes, generating sampling points, and finding out the number of sampling points in the hidden terminal coverage. The execution time of these four processes are t_1, t_2, t_3 and t_4, respectively. The fourth item occupies most of the execution time. Therefore, the execution time for one trial is

$$T_1 = t_1 + t_2 + t_3 + t_4 \approx t_4 \approx M_e^k U_t \tag{23}$$

where U_t represents the time to judge whether a sampling point is in the hidden terminal coverage. U_t is regarded as a

constant. M_e^k is different in each trial. The average number of sampling points for one trial is

$$M_{avg} = \frac{1}{n_e}\sum_{k=1}^{n_e} M_e^k \tag{24}$$

Therefore, the execution time of n_e trials is written as follows:

$$T_{\sum} = n_e M_{avg} U_t \tag{25}$$

3.2.2 The impact of the fading channel

Ma et al. [24] derived the expression of *PDR* considering the impact of fading channel by converting d-D Poisson Euclidean distance ordered node distribution to 1-D Poisson distribution. This paper refers to the expression of *PDR* considering the impact of the fading channel in [24]. We write it as shown in Eq. (26).

$$PDR_F(r) = e^{-\beta C_d (r^d - A)} \tag{26}$$

where r is the receiving range from the sender, β is the density of nodes, and

$$C_d = \begin{cases} \dfrac{\pi^{d/2}}{(d/2)!}, & \text{for even } d \\ \dfrac{\pi^{(d-1)/2} 2^d (\frac{d-1}{2})!}{d!}, & \text{for odd } d \end{cases}$$

and

$$A = \int_{w=0}^{w=r^d} \left[1 - \frac{m^m}{\Gamma(m)} \int_0^{(\sqrt[d]{w}/R)^\gamma} z^{m-1} e^{-mz} dz\right] dw$$

The overall *PDR* can be expressed as the following form.

$$PDR(r) = PDR_H(r) \times PDR_F(r) \tag{27}$$

3.3 *PRR* evaluation

PRR is the proportion of nodes receiving successfully in the total receiving nodes within the receiving range r from the sender. The total number of nodes in the receiving range is the product of the density of the nodes β and the size of the receiving area. We have derived the probabilities *NRP*s of individual node successfully receiving a packet from the sender. Because the average number of nodes within an incremental coverage dx is βdx, and the average number of nodes in dx that successfully receive the packet from the sender equals $NRP(x)\beta dx$. Therefore, the average number of nodes that receive the packet successfully over the receiving range r $(0 < r \le R)$ from the sender is equal to the integration of the *NRP* of all nodes within an incremental range. Therefore, the general expression of *PRR* is as follows:

$$PRR(r) = \frac{d}{r^d}\int_0^r NRP(x) x^{d-1} dx \tag{28}$$

4 Multi-parameter optimization scheme

4.1 Optimization problem definition

The QoS constraint transmission capacity (*TC*) [38] is defined as the number of nodes (N_{ROI}) in the region of interest (ROI) of the sender times the maximum beacon generation rate (λ) at which each source node transmits with optimized communication settings for a specific application such that the awareness of its one-hop surrounding nodes can be achieved with the required QoS. As the N_{ROI} would not change in a short time, the problem of maximizing the *TC* could be transferred to get the highest beacon generation rate λ_{max}. At the same time, choosing a bigger λ is not always good because the probability of packet collision would increase and then reduce the reliability of the network, such as *PRR*. Thus, the multi-parameter optimization problem could be formulated as follows:

$$\begin{aligned} \lambda_{max} &= \text{argmax } TC(N_{ROI}, \lambda) \\ &\text{subject to } PRR(\lambda, W, R_d) \ge \Delta \end{aligned} \tag{29}$$

where W is the back-off window size, R_d represents data rate, and Δ is the *PRR* threshold which stands for the application reliability requirements.

4.2 Optimization algorithm based on BBPSO

According to the definition of the optimization problem, a relatively high reliability threshold should be guaranteed first [39], then it is worthwhile to maximize the λ. Because there are couples of parameters that could be adjusted and their combination would be enormous or even infinite, so it is necessary to apply a heuristic algorithm to solve the problem. We apply BBPSO, which is different from the conventional PSO of [26]. Compared with other heuristic-based algorithms (such as, conventional PSO [40], simulated annealing [41], ant colony optimization [42] and so on), there is no any parameters that need to be predefined in BBPSO [43], which makes the algorithm less intuitive.

In this paper, we consider three transmission parameters and combine their value into a tuple (λ, W, R_d), which could be treated as a point in the solution space ($\lambda \in [5, 40]$ Hz, $W \in [15, 1023]$ μ s, $R_d \in [3, 54]$ Mbps) [26]. It is necessary to check whether *PRR* can be satisfied

first via randomly setting several points [26]. If there is a *PRR* higher than the threshold Δ, then maximize λ. But if no *PRR* is higher than Δ, it indicates that the system cannot meet the QoS requirements of the application. Then other measures should be adopted beyond the scope of this paper.

The iteration functions of BBPSO are show below,

$$\begin{aligned} &\boldsymbol{X}_i^{(k+1)} = N(\mu, \sigma_i^2); \quad \mu_i = (\boldsymbol{X}_{i,pbest}^{(k)} + \boldsymbol{X}_{gbest}^{(k)})/2 \\ &\sigma_i = |\boldsymbol{X}_{(i,pbest)}^{(k)} - \boldsymbol{X}_{gbest}^{(k)}| \end{aligned} \tag{30}$$

where N represents the Gaussian distribution, $\boldsymbol{X}_i^{(k)}$ is the ith particle (combination of (λ, W, R_d)) at kth iteration, the $\boldsymbol{X}_{i,pbest}^{(k)}$ is the best historical location of the ith particle and $\boldsymbol{X}_{gbest}^{(k)}$ is the best historical global solution. Each iteration selects a set of particles that satisfy the condition $PRR > \Delta$, then the particles in this set compare their λ with $\boldsymbol{X}_{i,pbest}^{(k)}$ and $\boldsymbol{X}_{gbest}^{(k)}$. If the λ is bigger in this set, update $\boldsymbol{X}_{i,pbest}^{(k)}$ and $\boldsymbol{X}_{gbest}^{(k)}$. Algorithm 2 shows the multi-parameter optimization process based on BBPSO.

Algorithm 2 Multi-parameter optimizing process

Input: $\Delta, \beta, E[PA], T_H, \delta, DIFS$.
Output: $\boldsymbol{X}$ with the biggest λ, and $PRR(\boldsymbol{X}) \geq \Delta$.

for each particle $\boldsymbol{X}$ **do**
  $\boldsymbol{X} \leftarrow \text{rand}(\lambda_{\boldsymbol{X}}, W_{\boldsymbol{X}}, R_{d\boldsymbol{X}})$; $\boldsymbol{X}_{pbest} \leftarrow$ None
end for
$\boldsymbol{X}_{gbest} \leftarrow$ None
for each round of iteration **do**
  for each particle $\boldsymbol{X}$ **do**
    Calculate packet reception ratio $PRR(\boldsymbol{X})$
    if $\boldsymbol{X}_{pbest} =$ None and $PRR \geq \Delta$ **then**
      $\boldsymbol{X}_{pbest} \leftarrow \boldsymbol{X}$
    end if
  end for
  for each $\boldsymbol{X}$ in $\{\text{particles}|PRR(\boldsymbol{X}) \geq \Delta\}$ **do**
    if $\boldsymbol{X}_{gbest} =$ None **then**
      $\boldsymbol{X}_{gbest} \leftarrow \boldsymbol{X}$
    end if
    if $\lambda_{\boldsymbol{X}} > \lambda_{\boldsymbol{X}_{gbest}}$ **then**
      $\boldsymbol{X}_{gbest} \leftarrow \boldsymbol{X}$
    end if
    if $\lambda_{\boldsymbol{X}} > \lambda_{\boldsymbol{X}_{pbest}}$ **then**
      $\boldsymbol{X}_{pbest} \leftarrow \boldsymbol{X}$
    end if
  end for
  for each particle $\boldsymbol{X}$ **do**
    update position with Eq. (30)
  end for
end for

5 The experimental validation

We have performed numerous experiments. For compactness of presentation, a brief outline of the experiment schemes and the results are discussed below.

5.1 Experimental settings

Table 4 presents the experimental environment, the programming languages with the version for implementing a function. During the theoretical computation, we write a MATLAB program to implement the fixed-point iteration process for calculating p_t. Another MATLAB program is used to implement the MC method evaluating $S_{\sum}^{g}$. Moreover, we use the Python programming language to calculate *NRP*s/*PDR*s/*PRR*s and implement the optimization algorithm based on BBPSO. Furthermore, we adopt NS2.35 to do simulation and analyze the *NRP*s/*PDR*s/*PRR*s from the trace files.

The experiment covers network situations from 1-D to 3-D. A 1-D broadcast area is assumed as a signal lane of 5000 m. The 2-D broadcast network is abstracted to a circular coverage with a radius of 1500 m. The 3-D broadcast network is realized in the spherical area with a range of 1000 m. We design three nodes densities with β (nodes/km^2) equal to 100, 150, and 200, for the 2-D case, and three nodes densities with β (nodes/km^3) equal to 120, 420, and 720, for the 3-D networks, respectively. We choose 25 receiving ranges with r equals 10 m to 490 m at an interval of 20 m to evaluate the reliability metrics. Then, 1000 trials are executed for each receiving range at every density. Table 5 lists the parameter settings for the MC method and wireless network. With the same communication settings, we compare *NRP*s/*PDR*s/*PRR*s from the computation and the NS2.35 simulation, and the computation of *PDR*s benefits the implementation of the MC method. Finally, we implement the multi-parameter optimization based on BBPSO.

5.2 Asymptotic behavior of S_{Σ}

In each trial, $S_{\sum}$ is obtained by generating uniformly distributed sampling points in the sample area SA. The more sampling points, the longer the execution time. Thus we need to minimize the number of sampling points. Figure 10 presents the comparisons of asymptotic behavior of $S_{\sum}$ in the 2-D scenario with a density of 100 (nodes/km^2). The relative errors ε_p are calculated with the confidence level 95.45%. It is not difficult to find that the larger the sampling area, the larger the relative error with the same

Table 4 Experimental platform, programming languages and tools

Module or languages	Model or function
Mainboard	MS-179B (100 Series/C230 Series Chipset Family-A152)
Hard drive	Samsung MZVLW128HEGR-00000 (128G/SSD)
CPU	Intel(R) Core(TM) i5-7300HQ CPU @2.50 GHz
Memory	8.0 GB (Samsung DDR4 2400 MHz)
OS	Ubuntu 18.04
Matlab 2016b	Implement fixed-point iteration for p_t and MC method for $S^g_{\sum}$
Python 2.7	Calculate *NRP*s/*PDR*s/*PRR*s theo- retically and implement optimization
NS2.35	Simulate a wireless broadcast network

Table 5 Parameter settings for the MC method and wireless networks

Parameters	Values
Predefined relative error e for ε_p	1%
Predefined relative error e for ε_s	1%
Confidence level	95.45%
Transmission range R	500 m
Carrier sensing range R_{cs}	500 m
Interference range R_{int}	500 m
Packet length PA	200 bytes
Data rate R_d	24 Mbps
Slot time t_{slot}	16 μs
PHY preamble T_{H1}	40 μs
Packet generation interval λ	0.1 s
MAC header T_{H2}	272 bits
PLCP header T_{H3}	4 μs
CW W-1	15
Path loss exponent γ	2
Fading parameter m if $x<50$ m	3
Fading parameter m if 50 m $\leq x<150$ m	1.5
Fading parameter m if $x\geq 150$ m	1

number of sampling points. Therefore, in each trial, we choose the smallest sampling area whose side length is shown as the Eq. (16). At the same time, the larger the receiving range, the smaller the relative error with the same number of sampling points. This can be inferred from Eq. (21). Moreover, we can find that the number of sampling points at which one can estimate $S_{\sum}$ accurately.

5.3 Asymptotic behavior of $\overline{S_{\Sigma}}$

Based on the experiment results, we plot the data-based histogram of $S_{\sum}$ from 1000 trials to better understand the characteristics of $H_{\sum}s$, then compare with the probability density function (PDF) of Gaussian distribution. Figure 11

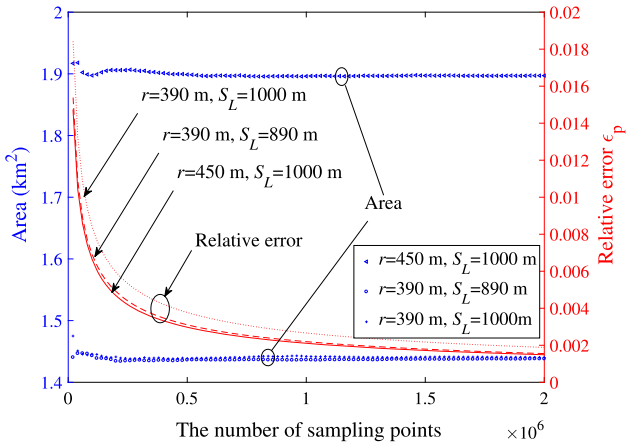

Fig. 10 Asymptotic behavior of $S_{\sum}$ and number of sampling points versus relative errors ε_p

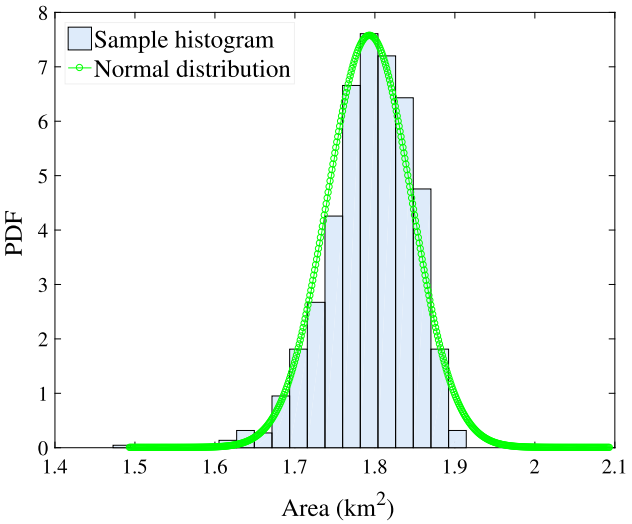

Fig. 11 Data-based histogram of $S_{\sum}s$ *versus* PDF of normal distribution ($r = 450$ m, $\beta = 100$ nodes/km^2)

gives the comparison results with the receiving range of 450 m and the nodes density of 100 nodes/km^2. Therefore, the random variable $S_{\sum}$ belongs to a normal distribution:

$$S_{\sum} \sim N(\mu, \sigma^2) \tag{31}$$

where $\overline{S_{\sum}}$ and $\sigma(S_{\sum})$ are unbiased estimation of μ and σ, respectively. The same distribution can also be observed for other receiving distances and nodes densities.

We examine the asymptotic properties of $\overline{S_{\sum}}$ with the increase in the trials number (see Fig. 12), to investigate the number of trials at which one can estimate $S^g_{\sum}$ accurately without fitting the data to a distribution. Figure 12 also presents the 2-sigma upper envelope curve and the 2-sigma lower envelope curve. As shown in Fig. 12, n_e denotes the number of trials with the given relative error of 0.01. Furthermore, Fig. 13 shows 965 observations with n_e trials for relative error of 0.01. Almost all observations fall within the 2-sigma confidence interval.

5.4 The number of sampling points and the number of trials

The more trials, the smaller the relative error and the longer the execution time. Figure 14 shows the number of trials with relative error ε_s of 0.01 for the 2-D case and 3-D scenario. We observe that the fewer trials are required with the increase in the receiving ranges and the nodes densities. In each trial, the number of sampling points is different for the same relative error because the nodes positions change. M_e^k represents the number of sampling points in the kth trial, and M_{avg} represents the average number of sampling points. M_e^k is 0 if there are no receiving nodes within the receiving range r. Based on these experiment results, Fig. 15 demonstrates M_{avg} against increasing receiving ranges and nodes densities for the 2-D case and 3-D scenario. It illustrates that as the receiving range increases

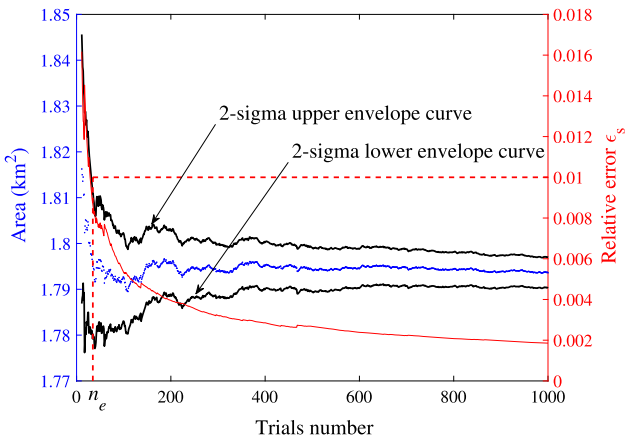

Fig. 12 Asymptotic behavior of $\overline{S_{\sum}}$ and relative error ε_s *versus* the number of trials ($r = 450$ m, $\beta = 100$ nodes/km^2)

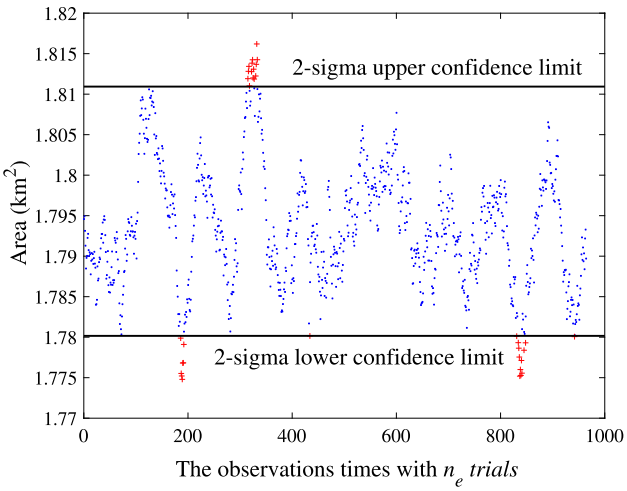

Fig. 13 Observations of $\overline{S_{\sum}}$ with n_e trials and relative error ε_s of 0.01 ($r = 450$ m, $\beta = 100$ nodes/km^2)

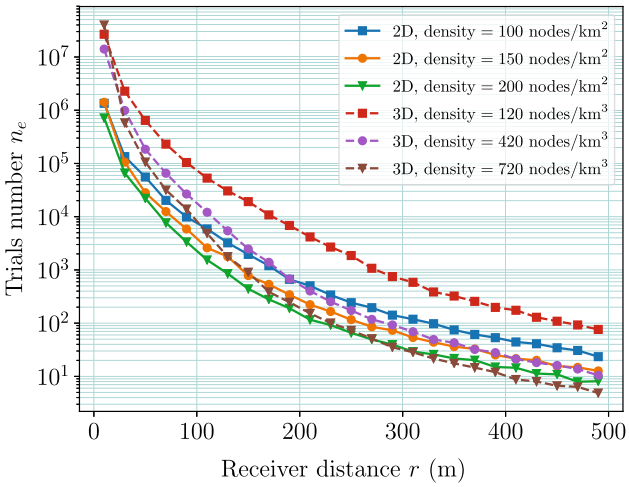

Fig. 14 Trials number with relative error ε_s of 0.01 in the 2-D and 3-D case

M_{avg} increases firstly, and soon, it decreases. Since the situation that there is no receiving node often occurs near the sender (e.g., less than 100), resulting in the number of sampling points being 0.

5.5 Execution time of the MC method

We record the base unit time U_t which represents the time for determining whether a sampling point is in $H_{\sum}$. We also count the total execution time of n_e trials for ε_p of 0.01 and ε_s of 0.01. When $\varepsilon_s > 0.01$, we perform another $(n_e - 1000)$ trials. Figures 16 and 17 plot U_t and the total execution time with increasing receiving distances in the 2-D case and 3-D scenario, respectively. The total execution time is $M_{avg} \times n_e \times U_t$. We witness that the total execution time

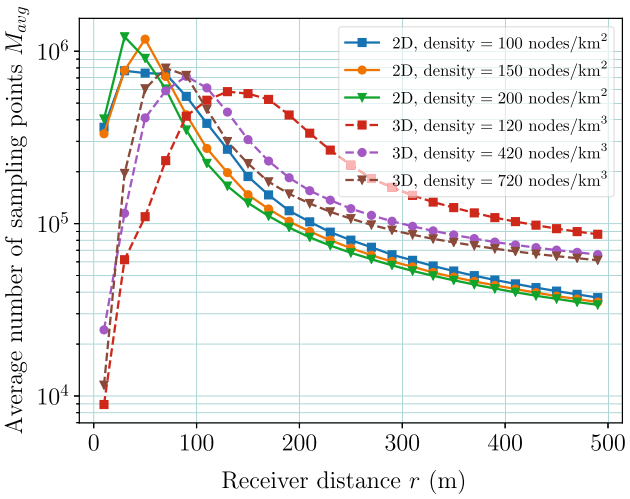

Fig. 15 Average number of sampling points with relative error ε_p of 0.01 in the 2-D and 3-D case

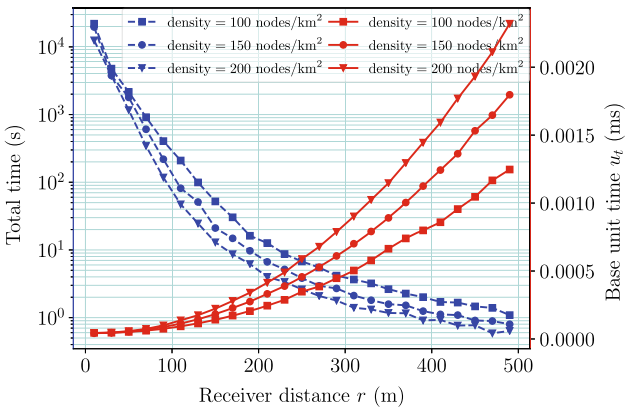

Fig. 16 U_t and the total execution time with ε_p of 0.01 and ε_s of 0.01 in the 2-D case

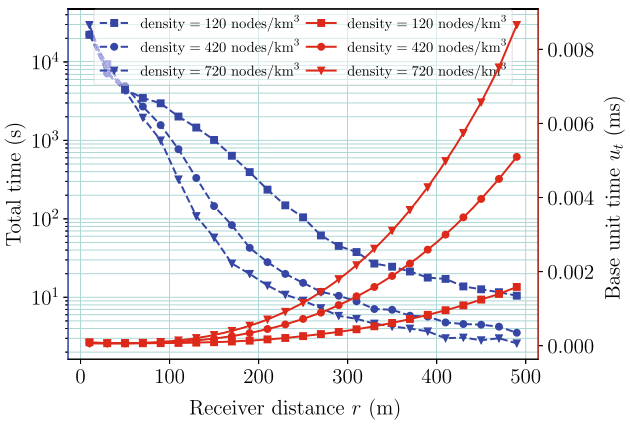

Fig. 17 U_t and the total execution time with ε_p of 0.01 and ε_s of 0.01 in the 3-D case

is mainly affected by the number of trials and the number of sampling points. U_t can be regarded as a constant compared to the number of trials and the number of sampling points.

Therefore, an evaluation for a near receiving distance and a low node density is usually the worst case. Decreasing the number of trials or the number of sampling points can speed up execution. The more the number of sampling points in each trial, the more accurate $S_{\sum}$ is. The Eq. (18) shows that the number of trials with ε_s of 0.01 is four times that with ε_s of 0.02. Properly increasing the relative error ε_s is a better solution for speeding up execution.

5.6 *NRP*/*PDR*/*PRR* results

We place 500 broadcast nodes in each defined network area. The six group results in Fig. 18 show the theoretical results and simulation results of *NRP*s/*PDR*s/*PRR*s with different receiving distances. In Fig. 18, the two data results with the slowest drop represent the *PRR*s from theoretical analysis and simulation. The two data results in the middle are the *NRP*s. The two fastest falling data results correspond to the *PDR*s. The data trends indicate that the farther the receiving nodes are from the sender, the smaller the probabilities of successfully receiving a packet. The analytical results expressed by the solid lines practically coincide with the simulation results represented by the symbols. Furthermore, *PDR*s go down dramatically when the receiving range goes up, *PDR*s are nearly zero when the distance is 300 m. Figures 19 and 20 compare the theoretical values and simulation values of *NRP*s/*PDR*s/*PRR*s in the 2-D and 3-D scenarios, respectively. The same conclusions can be obtained with the results of the 1-D case. Furthermore, we compute the relative errors (AE for average error and ME for maximum error) between the simulation results and the theoretical results, as shown in Table 6. These results illustrate that the analytical framework is accurate enough.

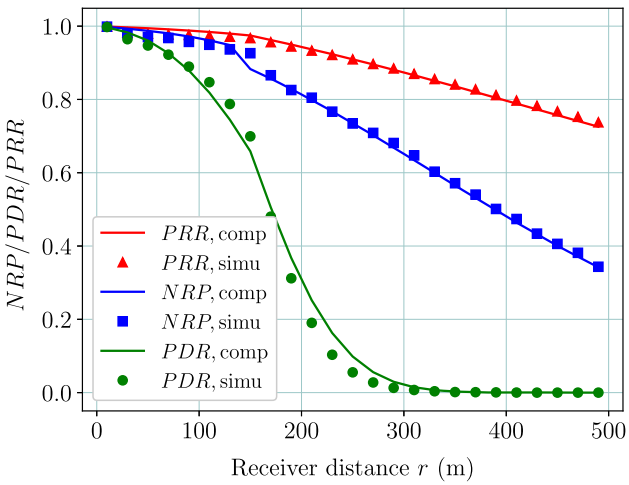

Fig. 18 *NRP*s/*PDR*s/*PRR*s of 1-D broadcast wireless networks

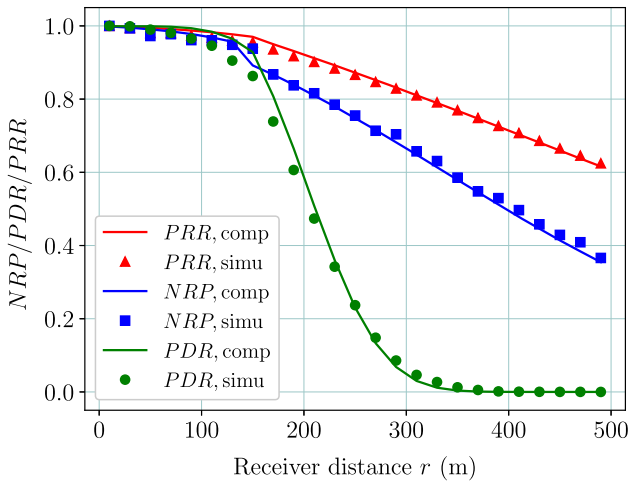

Fig. 19 *NRP*s/*PDR*s/*PRR*s of 2-D broadcast wireless networks

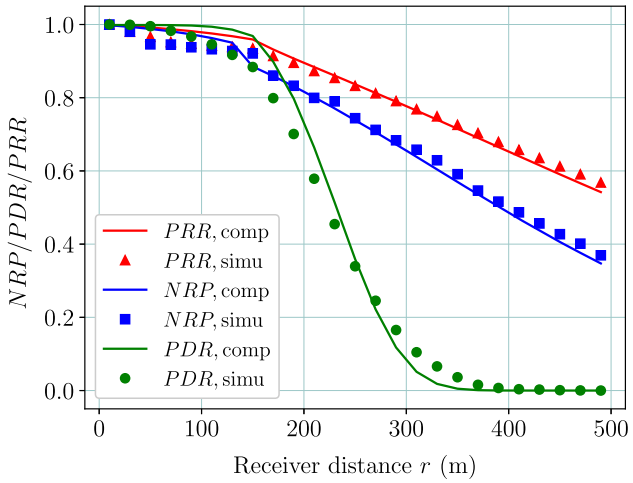

Fig. 20 *NRP*s/*PDR*s/*PRR*s of 3-D broadcast wireless networks

Table 6 The relative errors of *NRP*s/*PDR*s/*PRR*s between computation and simulation results

	1-D		2-D		3-D	
	AE (%)	ME (%)	AE (%)	ME (%)	AE (%)	ME (%)
NRP	0.91	4.32	1.14	4.58	1.84	4.22
PRR	0.73	1.47	0.75	1.70	1.64	3.52
PDR	1.84	6.16	1.94	6.91	3.38	7.95

5.7 Multi-parameter optimization results

We place 300 nodes in the 3-D spherical area with the radius of 500 m (573 nodes/km^3), and the range of ROI is set 300 m. Figure 21 illustrates the optimization process in the specific condition. The dotted line shows the *PRR*

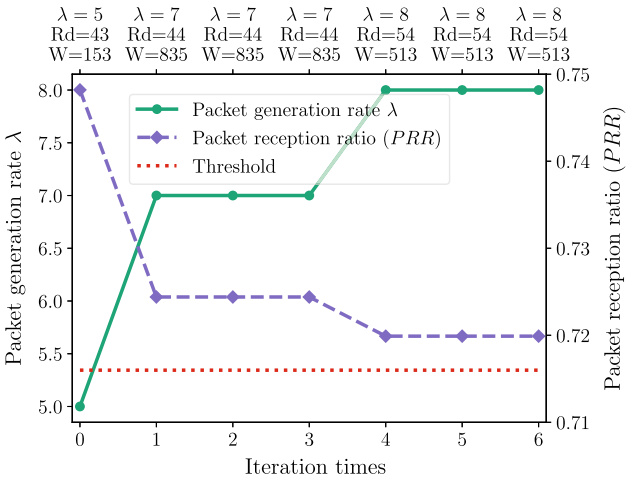

Fig. 21 Optimization process

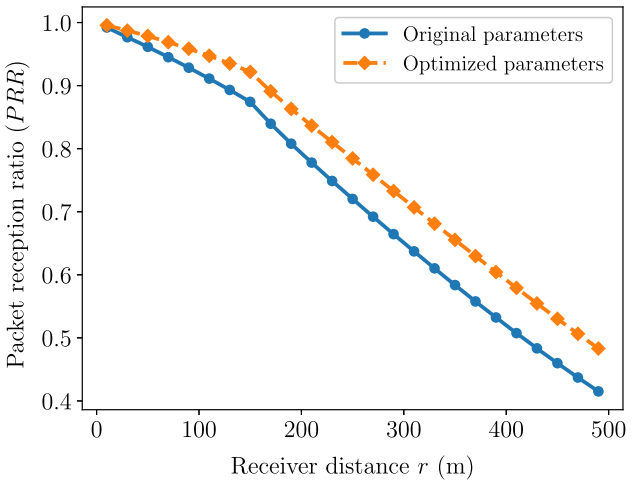

Fig. 22 Effect of optimization on *PRR*s

threshold. The parameters in each iteration are shown at the top, the solid line is the λ, the dashed line represents the *PRR*. We observe that the optimization algorithm can find the maximum λ in couples of iteration, and the *PRR*s are constrained over the threshold. The effect of the optimization is shown in Fig. 22. The dashed line shows the *PRR* with optimized parameters ($\lambda = 8$ Hz, $W = 513$ μs,$R_d = 54$ Mbps) and the solid line represents the *PRR* with original parameters ($\lambda = 10$ Hz, $W = 15$ μs,$R_d = 24$ Mbps). Moreover, the maximum improvement of the *PRR* reaches 10.4% when the distance equals 300 m.

6 Conclusions

In the present work, we programmed to compare the interference-based analytical method with the deterministic distance-based analytical method, both of which are used to estimate the reliability of IEEE 802.11 based 1-D broadcast

wireless networks. The results showed that the deterministic distance-based analytical model was reasonable. Then, we proposed a reliability analytical framework evaluating *NRP*s/*PDR*s/*PRR*s for *d*-D wireless broadcast networks. The framework took the fading channel and the hidden terminal problem into consideration. In the face of the major challenge caused by the complicated geometric characteristics of hidden terminal coverage in high dimensions, this paper proposed a mathematical approach to calculate the size of the hidden terminal coverage affecting *NRP* so that the general closed-form expression of *NRP*/*PRR* can be derived. At the same time, this paper adopted the MC method to solve the size of general hidden terminal coverage affecting *PDR*, which is an irregular area and changes with different scenarios, eliminating the key difficulty of *PDR* derivation. Finally, we introduced the multi-parameter optimization scheme based on BBPSO to ensure reliability, as well as maximize the transmission capacity.

We analyzed the effectiveness and accuracy of the MC method experimentally. The results illustrated that the number of trials and the number of sampling points would decrease with the receiving distances and the nodes densities. For the worst-case with small receiving distance and low nodes density, we can appropriately reduce the number of trials to improve efficiency. We conducted cross-validation experiments for 1-D/2-D/3-D wireless broadcast scenarios between the theoretical analysis and NS2.35 simulation. The results showed that the analytical results were consistent with the statistical results of the simulation. We also witnessed that the multi-parameter optimization scheme can find the optimum settings for the network based on the feedback of the analytical framework. The above study is useful to improve the performance of wireless broadcast networks based on IEEE 802.11 in the presence of fading and hidden terminals.

Acknowledgements We thank anonymous reviewers for their invaluable comments and suggestions on improving this work. This work is supported by the National Natural Science Foundation of China (NSFC) (Grant No. 61572150), and Central Fund of Dalian University of Technology (No. DUT17RC(3)097).

Appendix A *PDR*/*PRR* results of the interference-based model and the deterministic distance-based model

Figures 23, 24, 25, 26, 27, 28, 29 and 30 present *PDR*/*PRR* results of the interference-based model and the deterministic distance-based model with the data rate of 3 Mbps, 6 Mbps, 12 Mbps, and 24 Mbps. *PRR* results show the same behavior with *NRP* in Sect. 2.4. We witness that *PDR*s are almost identical in the low-to-medium density

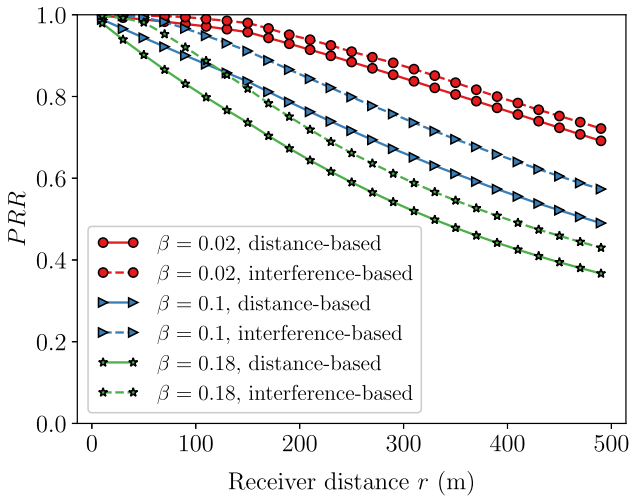

Fig. 23 *PRR* comparisons of the two models with the data rate of 3 Mbps

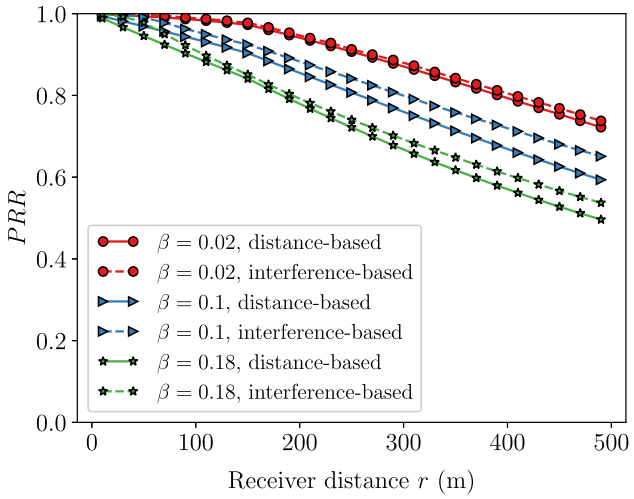

Fig. 24 *PRR* comparisons of the two models with the data rate of 6 Mbps

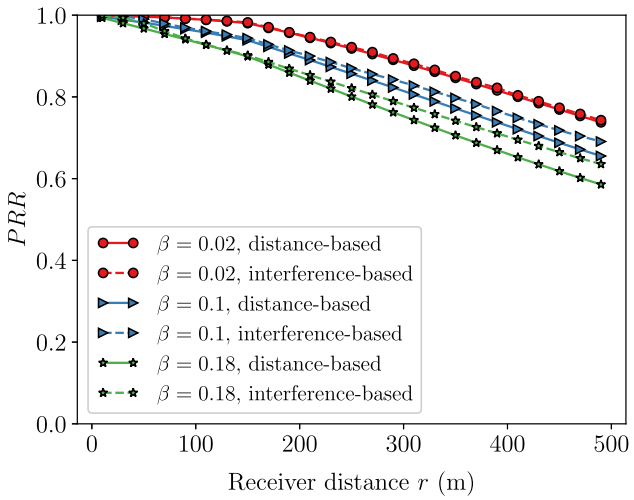

Fig. 25 *PRR* comparisons of the two models with the data rate of 12 Mbps

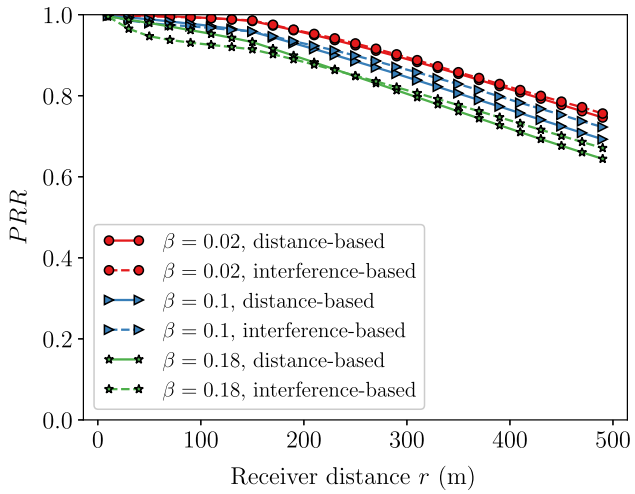

Fig. 26 *PRR* comparisons of the two models with the data rate of 24 Mbps

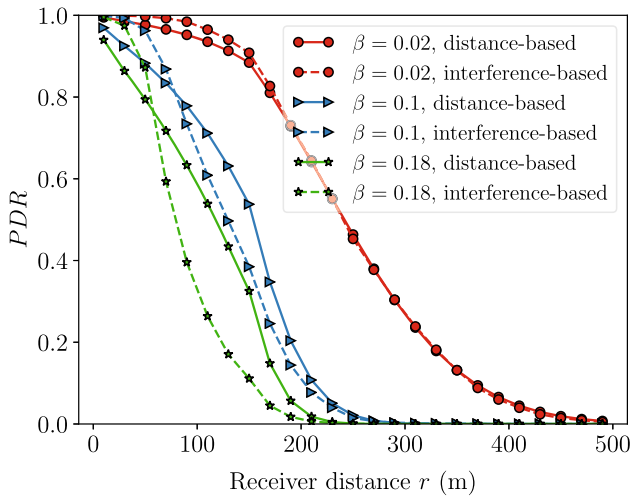

Fig. 27 *PDR* comparisons of the two models with the data rate of 3 Mbps

at each data rate. When the density increases, the deterministic distance model obtains better *PDR*s. This is because that the hidden terminals beyond the interference range in the deterministic distance-based analytical model do not be considered. But in the interference-based model, they can also lead to reception failure. At the same time, the definition of *PDR* shows that it is the most stringent evaluation metric which requires that a packet is received successfully by all neighbors. Therefore, the phenomenon happens.

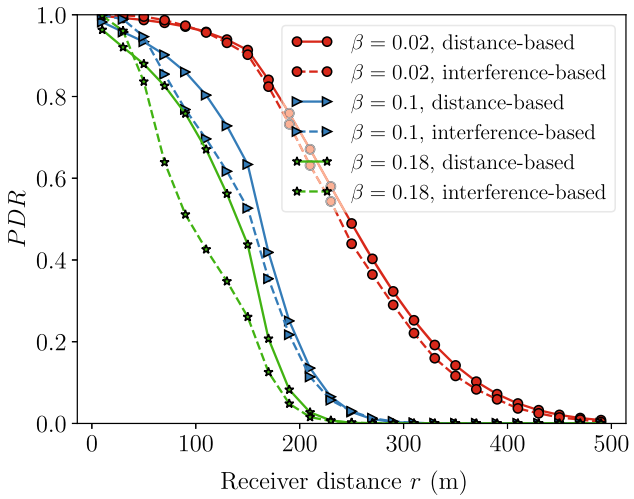

Fig. 28 *PDR* comparisons of the two models with the data rate of 6 Mbps

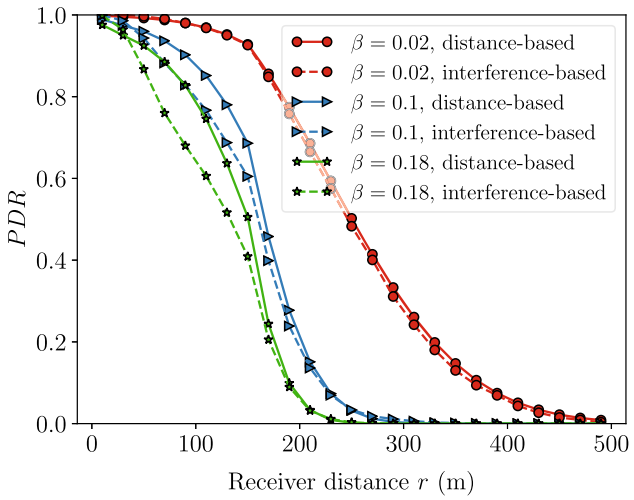

Fig. 29 *PDR* comparisons of the two models with the data rate of 12 Mbps

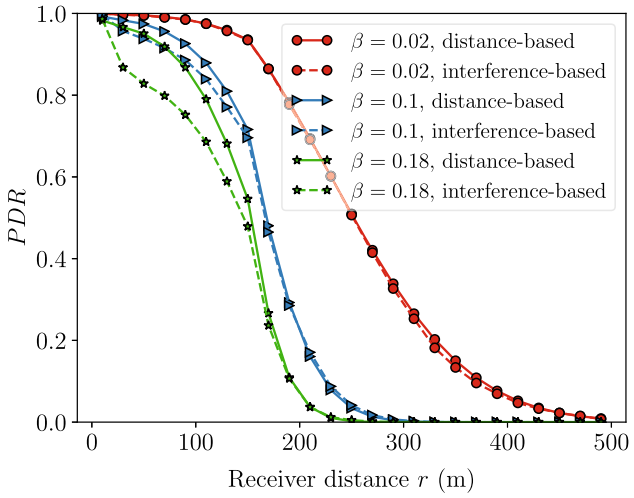

Fig. 30 *PDR* comparisons of the two models with the data rate of 24 Mbps

References

1. FallahHoseini, M., & Rafeh, R. (2018). Proposing a centralized algorithm to minimize message broadcastingenergy in wireless sensor networks using directional antennas. *Applied Soft Computing*, *64*, 272–281.
2. Ma, X., Zhang, J., Yin, X., & Trivedi, K. S. (2012). Design and analysis of a robust broadcast scheme for VANET safety-related services. *IEEE Transactions on Vehicular Technology*, *61*(1), 46–61.
3. He, J., Tang, Z., Fan, Z., & Zhang, J. (2018). Enhanced collision avoidance for distributed LTE vehicle to vehicle broadcast communications. *IEEE Communications Letters*, *22*(3), 630–633.
4. Gupta, L., Jain, R., & Vaszkun, G. (2016). Survey of important issues in UAV communication networks. *IEEE Communications Surveys & Tutorials*, *18*(2), 1123–1152.
5. Pan, C., Yin, C., Beaulieu, N. C., & Yu, J. (2019). 3D UAV placement and user association in software-defined cellular networks. *Wireless Networks*, *25*(7), 3883–3897.
6. Akyildiz, I., Su, W., Sankarasubramaniam, Y., & Cayirci, E. (2002). Wireless sensor networks: A survey. *Computer Networks*, *38*(4), 393–422.
7. Doumi, T., Dolan, M. F., Tatesh, S., Casati, A., Tsirtsis, G., Anchan, K., et al. (2013). LTE for public safety networks. *IEEE Communications Magazine*, *51*(2), 106–112.
8. Feickert, A. (2009). The Army's future combat system (FCS): Background and issues for congress. Library of congress Washington DC congressional research service.
9. Ma, X., Yin, X., & Trivedi, K. S. (2012). On the reliability of safety applications in VANETs. *International Journal of Performability Engineering*, *8*(2), 115–130.
10. Torrent-Moreno, M., Mittag, J., Santi, P., & Hartenstein, H. (2009). Vehicle-to-vehicle communication: Fair transmit power control for safety-critical information. *IEEE Transactions on Vehicular Technology*, *58*(7), 3684–3703.
11. Ma, X., Zhang, J., & Wu, T. (2011). Reliability analysis of one-hop safety-critical broadcast services in VANETs. *IEEE Transactions on Vehicular Technology*, *60*(8), 3933–3946.
12. Ye, F., Yim, R., Roy, S., & Zhang, J. (2011). Efficiency and reliability of one-hop broadcasting in vehicular ad hoc networks. *IEEE Journal on Selected Areas in Communications*, *29*(1), 151–160.
13. Yin, X., Ma, X., & Trivedi, K. S. (2013). An interacting stochastic models approach for the performance evaluation of DSRC vehicular safety communication. *IEEE Transactions on Computers*, *62*(5), 873–885.
14. Hassan, M. I., Vu, H. L., & Sakurai, T. (2011). Performance analysis of the IEEE 802.11 MAC protocol for DSRC safety applications. *IEEE Transactions on Vehicular Technology*, *60*(8), 3882–3896.
15. Hafeez, K. A., Zhao, L., Ma, B., & Mark, J. W. (2013). Performance analysis and enhancement of the DSRC for VANET's safety applications. *IEEE Transactions on Vehicular Technology*, *62*(7), 3069–3083.
16. Ma, X., Yin, X., Wilson, M., & Trivedi, K.S. (2013). Mac and application-level broadcast reliability in vanets with channel fading. In *2013 international conference on computing, networking and communications* (pp. 756–761).
17. Tong, Z., Lu, H., Haenggi, M., & Poellabauer, C. (2016). A stochastic geometry approach to the modeling of DSRC for vehicular safety communication. *IEEE Transactions Intelligent Transportation Systems*, *17*(5), 1448–1458.
18. Ni, M., Pan, J., Cai, L., Yu, J., Wu, H., & Zhong, Z. (2015). Interference-based capacity analysis for vehicular ad hoc networks. *IEEE Communications Letters*, *19*(4), 621–624.
19. Ma, X., Lu, H., Zhao, J., Wang, Y., Li, J., & Ni, M. (2017). Comments on interference-based capacity analysis of vehicular ad hoc networks. *IEEE Communications Letters*, *21*(10), 2322–2325.
20. Goldsmith, A. (2005). *Wireless communications*. Cambridge: Cambridge University Press.
21. Chun, Y. J., Colombo, G. B., Cotton, S. L., Scanlon, W. G., Whitaker, R. M., & Allen, S. M. (2017). Device-to-device communications: A performance analysis in the context of social comparison-based relaying. *IEEE Transactions on Wireless Communications*, *16*(12), 7733–7745.
22. Dousse, O., Baccelli, F., & Thiran, P. (2005). Impact of interferences on connectivity in ad hoc networks. *IEEE/ACM Transactions on Networking*, *13*(2), 425–436.
23. Ma, X., & Trivedi, K. S. (2016). Reliability and performance of general two-dimensional broadcast wireless network. *Performance Evaluation*, *95*, 41–59.
24. Ma, X., & Butron, G. (2015). On the reliability in d-dimensional broadcast wireless networks. In *International conference on computing, networking and communications* (pp. 957–961).
25. Chen, X., Oorjitham, J., & Ma, X. (2011). On the two-dimensional coverage area in broadcast ad hoc networks. In *2011 IFIP wireless days* (pp. 1–5).
26. Zhao, J., Wu, Z., Wang, Y., & Ma, X. (2019). Adaptive optimization of qos constraint transmission capacity of vanet. *Vehicular Communications*, *17*, 1–9.
27. Xu, K., Gerla, M., Bae, S., & et al. (2002). How effective is the IEEE 802.11 RTS/CTS handshake in ad hoc networks? In *GlobeCom* (pp. 72–76).
28. Bianchi, G., Fratta, L., & Oliveri, M. (1996). Performance evaluation and enhancement of the CSMA/CA MAC protocol for 802.11 wireless LANs. In *Proceedings of IEEE international symposium on personal, indoor, and mobile communications* (pp. 392–396).
29. Ma, X., Yin, X., Butron, G., Penney, C., & Trivedi, K. S. (2013). Packet delivery ratio in k-dimensional broadcast ad hoc networks. *IEEE Communications Letters*, *17*(12), 2252–2255.
30. Tong, Z., Lu, H., Haenggi, M., & Poellabauer, C. (2016). A stochastic geometry approach to the modeling of dsrc for vehicular safety communication. *IEEE Transactions on Intelligent Transportation Systems*, *17*(5), 1448–1458.
31. Yao, Y., Rao, L., & Liu, X. (2013). Performance and reliability analysis of IEEE 802.11p safety communication in a highway environment. *IEEE Transactions on Vehicular Technology*, *62*(9), 4198–4212.
32. Killat, M., & Hartenstein, H. (2009). An empirical model for probability of packet reception in vehicular ad hoc networks. *EURASIP Journal on Wireless Communications and Networking*, *2009*, 1–12.
33. Rappaport, T. S., et al. (1996). *Wireless communications: Principles and practice* (Vol. 2). Upper Saddle River, NJ: Prentice Hall PTR.
34. Li, S. (2011). Concise formulas for the area and volume of a hyperspherical cap. *Asian Journal of Mathematics and Statistics*, *4*(1), 66–70.
35. Yin, X., Ma, X., & Trivedi, K. S. (2013). Channel fading impact on multi-hop DSRC safety communication. In *Proceedings of the*

16th ACM international conference on Modeling, analysis and simulation of wireless and mobile systems (pp. 443–446).
36. Pasupathy, R. (2010). Generating homogeneous Poisson processes. In *Wiley encyclopedia of operations research and management science* (pp. 1–6). Hoboken, NJ, USA: Wiley.
37. Dubi, A. (2000). *Monte Carlo applications in systems engineering*. New York: Wiley.
38. Lu, N., & Shen, X. S. (2014). *Capacity analysis of vehicular communication networks*. Berlin: Springer.
39. Sander Frigau, M. (2013). Cross-layer transmit power and beacon rate adaptation for vanets. In *Proceedings of the third ACM international symposium on design and analysis of intelligent vehicular networks and applications* (pp. 129–136).
40. Kennedy, J., & Eberhart, R. (1995). Particle swarm optimization. In *Proceedings of international conference on neural networks* (pp. 1942–1948).
41. Henderson, D., Jacobson, S. H., & Johnson, A. W. (2003). The theory and practice of simulated annealing. In F. Glover, G. A. Kochenberger (Eds.), *Handbook of metaheuristics* (pp. 287–19). Boston: Springer.
42. Dorigo, M., & Stützle, T. (2003). The ant colony optimization metaheuristic: Algorithms, applications, and advances. In F. Glover, G. A. Kochenberger (Eds.), *Handbook of metaheuristics* (pp. 250–285). Boston: Springer.
43. Kennedy, J. (2003). Bare bones particle swarms. In *Proceedings of the 2003 IEEE swarm intelligence symposium* (pp. 80–87).

Jing Zhao received Ph.D. (2006) degree in Computer Science and Technology in Harbin institute of Technology of China. In 2010 she was with Department of Electrical and Computer Engineering at Duke University, Durham, NC, working as a Postdoc under supervision of Dr. Kishor Trivedi. She is currently a Professor in the School of Software Technology, Dalian University of Technology of China. Her research interests include reliability engineering, software aging theory, and dependability modeling.

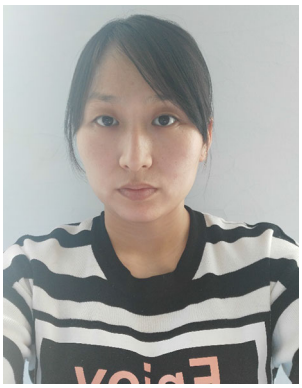

Zhijuan Li received the M.S. degree at the School of Computer Science and Technology, Harbin Engineering University, Harbin, China, in 2013. From 2013 to 2016, she was a Software Engineer with Harbin Yuguang Virtual Network Technology Co., Ltd, China. She is currently working toward the Ph.D. degree with the School of Computer Science and Technology, Harbin Engineering University. Her research interests include vehicular ad hoc network and fog computing.

Yanbin Wang received the Ph.D. degree from the Industrial Engineering Department, Harbin Institute of Technology of China, in 2007. He is currently an Associate Professor in the Department of Industrial Engineering, School of Mechatronics Engineering, Harbin Institute of Technology of China. His research interests include quality management, scheduling, optimization ,physical layer and MAC layer of vehicular ad hoc wireless networks.

Zhuofei Wu received the B.E. and M.E. degrees in College of Ship Building Engineering at Harbin Engineering University, China. Currently, He is working toward the Ph.D. degree in Computer Science and Technology at Harbin Engineering University, China. His research interests include reliability evaluation and performance optimization of vehicle ad-hoc network.

Xiaomin Ma (M'03–SM'08) received the B.E. degree from Anhui University, Hefei, China; the M.E. degree in Electrical Engineering from the Beijing University of Aerospace and Aeronautics, Beijing, China; and the Ph.D. degree in Information Engineering from the Beijing University of Posts and Telecommunications, Beijing, China, in 1999. From 2000 to 2002, he was a Postdoctoral Fellow with the Department of Electrical and Computer Engineering, Duke University, Durham, NC, USA. He is currently a Professor with the Department of Engineering, Oral Roberts University, Tulsa, OK, USA. His research interests include stochastic modeling and analysis of computer and communication systems; physical layer and medium-access layer of vehicular ad hoc wireless networks; computational intelligence and its applications to coding, signal processing, and control; and quality of service and call admission control protocols in wireless networks.

Yue Zhao received the B.S. degree in communication engineering in 2006 from the North China Institute of Science and Technology, Langfang, China, and the Ph.D. degree in information and communication systems in 2012 from Southwest Jiaotong University, Chengdu, China. From September 2010 to September 2011, he was a Visiting Student in the Department of Electrical and Computer Engineering, University of Florida. He is currently a Senior Engineer of science and technology on communication security